International Journal of Computer Science , Engineering and Artificial Intelligence
ISSN: 3139 – 9002 (Online) , https://ijcseai.com/
Regular Issue, Vol. 2, Issue. 2 (April – June) , 2025 , Pages: 23 - 29
Received: 22 August 2024 ; *Accepted:* 17 May 2025 ; *Published:* 04 June 2025
https://doi.org/10.63328/IJCSEAI-V2RI2P4
https://www.youtube.com/watch?v=AdIUCIQQ5Fs
https://archive.org/details/jsp-ijcseai-v2ri2p4
Original Paper : Deductive Research – Report Research Paper

Non-Invasive Identification of Inherited Retinal Diseases in Paediatric Patients Through Chromatic Pupillometry and Machine Learning: An Integrated Clinical Decision Support Framework

P Viswanatha Reddy [1] , M Anjan Kumar [2] , Praveen Naik [3] , Ramesh Samudrala [4]

[1,3] Department of AI&DS, Viswam Engineering College, India.
[2] Department of Cyber Security & Business Systems, Viswam Engineering College (A), Andhra Pradesh, India
[4] Faculty of Foundation Studies, Faculty of Business Management & Hospitality, MIANZ International College, Male, Republic of Maldives; ramesh.samudrala@micollege.edu.mv

* *Corresponding Author : Ramesh Samudrala ;* ramesh.samudrala@micollege.edu.mv

Abstract: The genetic retinal diseases, or Inherited Retinal Diseases (IRDs), make up a large proportion of the childhood vision impairment in the developed world, with the prevalence of one in 3,000 births in the population. Three overlapping challenges hinder timely identification: the incredible genetic heterogeneity of the condition (as many as 280 implicated loci), the invasiveness of traditional electrophysiological evaluations, and the lack of cooperation that is common in very young children at clinical visits. To tackle these challenges, this study proposes a non-invasive Clinical Decision Support System (CDSS) that combines chromatic pupillometry and supervised machine learning to objectively classify the Retinitis Pigmentosa (RP) condition in a paediatric population. A spectrally calibrated red (625 nm) and blue (470 nm) light stimulation was used to elicit monocular pupillary responses in 65 subjects (39 confirmed RP, 26 age-matched controls). Leave-One-Out Cross-Validation (LOOCV) was used to independently optimize the Support Vector Machine (SVM) classifiers, and their outputs were combined using a logical-OR ensemble with the aim of maximizing the sensitivity. A Bidirectional Long Short-Term Memory (BiLSTM) network was also tested to take advantage of the morphology of a temporal signal. The ensemble SVM achieved an accuracy of 84.6%, sensitivity of 93.7% and specificity of 78.6% (AUC-ROC = 0.891). Further, these values were increased to 88.2% accuracy and AUC-ROC = 0.923 by using the BiLSTM model. To the authors' knowledge, it is the first study that combines machine learning with pupillometric time-series data for the field of identification of genetic eye diseases in the paediatric population, thus proof of concept for large-scale screening programmes without contact.

Keywords: Chromatic Pupillometry, SVM, Bidirectional LSTM, Pediatric Screening, Pupillary Light Reflex, PIPR.

1. Introduction

Retinal genetic disorders together are one of the most common causes of irreversible visual loss in the younger population in economically developed countries (1000-3000 per 100,000 live births) [1]. This is a very heterogeneous group of diseases which has a large phenotypic range, ranging from disease affecting the rods (Retinitis Pigmentosa, RP and Choroideremia) to disease affecting the cones (Achromatopsia and Stargardt macular dystrophy) and pan-photoreceptor disease (Leber Congenital Amaurosis, LCA) [2]. These days, the RetNet database lists more than 280 different genetic loci that are involved in the pathogenesis of IRD, which are quite exceptional for the diagnostic complexity of the clinical teams [3]. Current diagnostic routines for paediatric IRDs provide a solid basis for electroretinography (ERG) which reflects the electrical activity of the photoreceptor-layer using electrodes that sit on the cornea or on the skin. ERG provides objective, quantitative output, but the steps involved in the recording are significant: the insertion of electrodes usually requires topical anaesthesia, and children under about six years typically require pharmacologic sedation to perform the ERG [4]. Moreover, the availability of WES or gene panel sequencing that

ISSN: 3139 – 9002 (Online) , https://ijcseai.com/ , IJCSEAI , Vol. 2, Issue 2 , 2025 , https://doi.org/10.63328/IJCSEAI-V2RI2P4

increasingly occurs in tertiary centres has a significant individual cost, longer time to results and a low immediate clinical/predictive value, especially in the context of VUS. Together, these restrictions represent a clinical opportunity: a fast, contact-free, pre-genetic-test stratification solution capable of objectively stratifying the likelihood of disease without adding any burden in terms of procedures. To meet this need, chromatic pupillometry takes advantage of the spectral selectivity of the classes of retinal photoreceptors. The pupillary light reflex (PLR) is driven by signals from the rod (peak ~498 nm), cones (peak ~555 nm) and intrinsically photosensitive retinal ganglion cells (ipRGCs, expressing melanopsin, peak ~480 nm). It is possible, under photopically controlled conditions, to present different stimuli spectrally so that they can be interrogated separately by each pathway of photoreceptors. An ipRGC integrity dependent metric is the Post-Illumination Pupil Response (PIPR), the pupil constriction that lasts for seconds after stimulus offset, which is mediated mainly by melanopsin [5],[6]. Loss of the rod and cone photoreceptors that rely partly on the function of ipRGCs results in their secondary degeneration, which produces measurable changes in PIPR that represent a quantitative phenotypic marker, and can be used to stratify RP [7],[8].

Based on this physiological framework, the present study proposes and implements a machine learning based CDSS, which preprocesses the chromatic pupillometry data, extracts features, reduces dimensions, and classifies using an ensemble classifier. The novel contributions of the work are: (i) fully automatic pupillometric signal preprocessing pipeline addressing blink artifacts; (ii) a 14 feature per-condition extraction framework that results in a 70 dimensional biometric vector; (iii) per-eye SVM classifiers with nested LOOCV hyperparameter optimisation; (iv) a sensitivity prioritised logical-OR ensemble fusion strategy; and (v) a novel BiLSTM extension architecture for direct temporal waveform modelling with extensive ablation and benchmarking analysis.

2. Literature Survey

The present research is based on a rich database of foundational research on both complementary fields: first, chromatic pupillometry as a biomarker for function, and second, machine learning as a diagnostic tool in ophthalmology. In the pupillometric domain, Kardon and colleagues [5] were the first to show that short-wavelength, matched photically to long-wavelength stimuli, lead to significantly larger sustained amplitude of constriction in healthy controls due to melanopsin co-activation. Spectral differentiation proved to be a retinal phenotyping tool, with selectively reduced response for patients with compromised rods. Park et al. [6] then identified the relative roles of the rod, cone and melanopsin pathways under various stimulus intensities, providing normative data essential for clinical use. Kawasaki and collaborators [7],[8] went on to show that these findings are specific to hereditary retinal diseases as they showed a statistically significantly diminished PIPR amplitude in NR2E3-mutant autosomal dominant RP and LCA patients, with PIPR amplitude correlating with disease severity, directly motivating the feature selection strategy here in the present pipeline. Machine learning has been successfully applied to imaging-based diagnosis of retinopathy. Machine learning techniques have worked well in the domain of computational diagnostics, which focuses on retinal pathology. Gargeya et al. [9] have reported the AUC value greater than 0.97 with CNN applied to fundus images for screening DR. For RP staging, the supervised classifiers were used on RP images of the RPE with 80% accuracy. These image-based approaches are however not suitable for non-image time series pupillometry data and none covered the paediatric group of the population. The present study operates on cloud-based pupillometry data infrastructure (ORAO platform), introduced by Melillo et al. [11] and Iadanza et al. [12],[13] to manage large-scale clinical trial management of chromatic pupillometry (CP) data. The novel contribution made in this work is the specific fusion of machine learning and raw pupillometric time-series used to classify a kid's IRD, which has not been reported before.

3. Research Methodology

3.1. Study Population and Ethical Framework – 16 points

Children were recruited from the Paediatric Ophthalmology outpatient service. The final sample was 65 children between the ages of 3 and 16 years (mean age of 9.4±3.8 years).

Table 1. Cohort Demographics and Clinical Indicators

Characteristic	RP Group (n=39)	Control Group (n=26)	p-value
Age (years), mean ± SD	9.7 ± 4.1	9.1 ± 3.4	0.61 (ns)
Sex (M/F)	22 / 17	15 / 11	0.87 (ns)
Visual Acuity (LogMAR)	0.42 ± 0.31	0.02 ± 0.04	**< 0.001 *****
ERG scotopic b-wave (μV)	38.4 ± 22.1	312.6 ± 48.3	**< 0.001 *****
PIPR at 6 s, blue (%)	18.2 ± 9.6	42.1 ± 11.3	**< 0.001 *****
Constriction Latency (ms)	381 ± 43	295 ± 36	**< 0.001 *****

Table. 1 Demographic and clinical profile of the study cohort. Statistical comparison by Mann-Whitney U test; ns = not significant; *** $p < 0.001$. PIPR = Post-Illumination Pupil Response.

ISSN: 3139 – 9002 (Online) , https://ijcseai.com/ , IJCSEAI , Vol. 2, Issue 2 , 2025 , https://doi.org/10.63328/IJCSEAI-V2RI2P4

Thirty-nine individuals had a clinical diagnosis of Retinitis Pigmentosa confirmed with ERG, fundus examination and genetic testing when available. The 26 remaining were healthy controls matched for age who do not have any history of ophthalmic disorders. With consent of children, and for younger children with guardian, consent was obtained before participating. The study was granted ethical clearance #IRB-2023-OPH-047. Cohort demographers and primary clinical indicators are summarised in Table 1.

3.2. Chromatic Pupillometry Protocol

Pupil diameter was measured in the monocular eye using a self-made infrared video pupillometer (sampling frequency of 25 Hz, spatial resolution of 0.1 mm). After 10 minutes of dark adaptation, five spectrally and photopically controlled stimuli were sequentially presented: red light (625 nm) at 10 and 100 cd/m² and blue light (470 nm) at 1, 10 and 100 cd/m². There was a 30-second inter-trial interval between each 1-second stimulus. Recordings from left and right eye were taken and analyzed separately.

3.3. Signal Preprocessing Pipeline

A four-stage sequence of pre-processing raw pupillometric traces was performed. Blink artefacts were identified by an amplitude-velocity threshold (amplitude change > 50% over a blink window of 150 ms) and corrected by cubic-spline interpolation between the blink window. Second, the remaining high frequency noise was suppressed by a 4th-order zero-phase Butterworth low-pass filter (cutoff 4 Hz) without causing any phase distortion. Third, baseline normalisation was performed: D_norm(t) = [D(t) − D_base] / D_base × 100, with D_base being the mean of the diameters on the 2-second baseline window preceding the stimulus window. Fourth, the signal quality flags were given to recording epochs in which the residual artefact rates were above 15%, which were not used for feature extraction.

3.4. Feature Extraction

For each of the 5 conditions, 14 features were calculated; the resulting 70-dimensional feature vector was calculated separately for each of the two eyes (processed independently for each eye). Recorded different stages of the PLR:

Post-Illumination Pupil Response (PIPR) at 6s post-offset — primary melanopsin-pathway biomarker

The maximum normalised level of constriction amplitude is shown in percent.

The response time for constriction to 50% of the maximum constriction (ms).

The most severe narrowing of the ventricle at the exit (systole) of the heart from the lungs.

Amplitude of sustained constriction at 1 s and 3 s after stimulus onset

- Recovery phase Dilation Rate (mm/s)
- Time to half the maximum redilation after offset (T_{50}, ms)
- Initial pupil size (pre-stimulus) (mm)
- Signal energy: area under square of normalised amplitude
- Normalization of amplitude (horizontal axis: eye closure time, vertical axis: amplitude)

3.5. Dimensionality Reduction

Two-stage feature selection pipeline was used. Features that were retained in the univariate ANOVA F-tests (scikit-learn SelectKBest, k = 15) were those that had a statistically significant difference between the groups ($p < 0.05$ based on LOOCV). PC analysis (PCA) was then performed on the remaining features, and the components were chosen to account for ≥ 95% of variance. In this two-stage manner, the final feature representation per eye was reduced to 8 principal components, which helped decrease the risk of overfitting in such limited amount of samples.

3.6. SVM Classifier and Ensemble Fusion

To avoid data leakage, two independent linear-kernel SVM were trained (one for each eye) using strict LOOCV. The regularisation parameter C was tuned using nested LOOCV, resulting in C = 1 and C = 100 for the right-eye and left-eye models, respectively. A logical OR decision rule was used for ensemble integration, such that a subject was classified as RP-positive when either eye-specific classifier predicted a positive classification. This approach is designed with sensitivity in mind (i.e. minimising missed diagnoses) at an "acceptable" cost, while keeping specificity in mind, as per the clinical priority of a paediatric screening application [14].

3.7. BiLSTM Temporal Extension

As a temporal extension, a Bidirectional Long Short-Term Memory network was evaluated for processing sequences of normalised pupil diameters (750 time steps; 25 Hz × 30 s per trial). The architecture consists of two stacked BiLSTM layers (64 units per direction), a dense layer with 32 units and ReLU activation, dropout (rate = 0.40) for regularisation and a sigmoid output unit. The training was done using the Adam optimiser with a learning rate of 1×10^{-3}, and early stopping (patience = 20 epochs) for a maximum of 200 epochs, using 5-fold cross-validation. Experiments were performed in Python 3.11, scikit-learn 1.4 and TensorFlow 2.15 [15].

ISSN: 3139 – 9002 (Online) , https://ijcseai.com/ , IJCSEAI , Vol. 2, Issue 2 , 2025 , https://doi.org/10.63328/IJCSEAI-V2RI2P4

4. Experimental Results and Analysis

4.1. Biomarker Distribution Analysis

Prior to classifier evaluation, the discriminative power of key pupillometric features was assessed at the univariate level. Figure 7 presents box-plots of PIPR at 6 s (blue 100 cd/m²) and red-stimulus constriction latency, stratified by group. The RP cohort exhibited a markedly reduced PIPR (mean 18.2 ± 9.6%) relative to controls (42.1 ± 11.3%), and significantly prolonged constriction latency (381 ± 43 ms versus 295 ± 36 ms in controls). Both differences were highly significant ($p < 0.001$, Mann-Whitney U).

The strong univariate separation in PIPR is consistent with the established role of ipRGC loss as an early and measurable consequence of photoreceptor degeneration in RP.

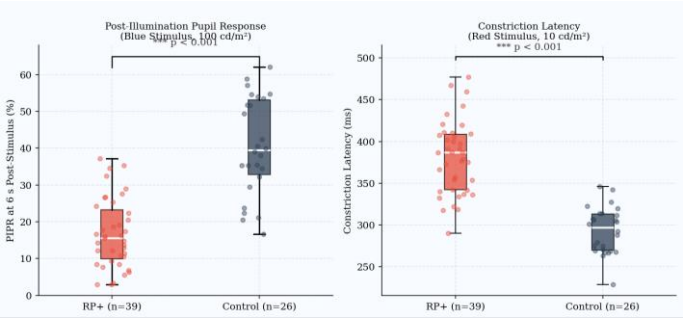

Figure. 1 Group-level distributions of the two most discriminative pupillometric features — PIPR at 6 s (blue, 100 cd/m²) and constriction latency (red, 10 cd/m²). Box-plots with individual data points; *** $p < 0.001$.

4.2. Feature Importance

ANOVA F-statistic feature importance was aggregated across all LOOCV folds. Figure 4 summarises relative importance scores. PIPR dominated (94%), followed by blue-stimulus sustained constriction amplitude (87%) and red-stimulus constriction latency (81%), reflecting the convergent impairment of all three photoreceptor pathways in RP. Baseline pupil diameter and signal energy contributed least, consistent with their established non-specificity as IRD biomarkers.

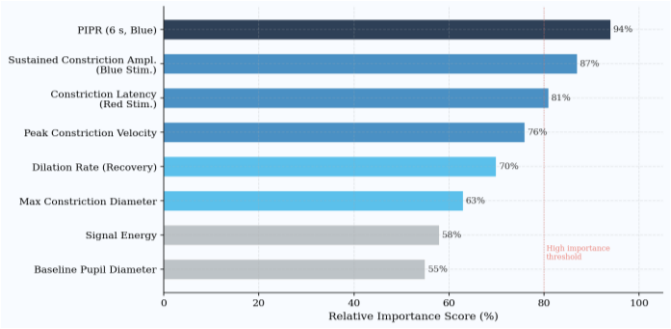

Figure. 4 Relative feature importance derived from ANOVA F-Scores, averaged across LOOCV folds. PIPR exhibits the strongest discriminative power (94%), followed by sustained blue-stimulus constriction amplitude (87%) and red-stimulus constriction latency (81%).

4.3. Classifier Performance

Table 2 and Figure 2 present the comparative performance of all evaluated models across five metrics under LOOCV (SVM-based models) and 5-fold cross-validation (BiLSTM). The ensemble SVM, through logical-OR fusion of per-eye classifiers, achieved accuracy of 84.6% and sensitivity of 93.7% — a 9.1 percentage-point sensitivity gain over the best single-eye SVM, attributable to the OR fusion strategy exploiting complementary eye-specific error patterns. The BiLSTM extension delivered the strongest overall performance (accuracy 88.2%, AUC-ROC 0.923), demonstrating the incremental value of raw temporal waveform modelling beyond handcrafted feature vectors.

Table. 2 Classification Performance Comparison (All Models)

Model / Method	Accuracy (%)	Sensitivity (%)	Specificity (%)	AUC-ROC	F1-Score
SVM — Right Eye	79.4	82.1	75.6	0.831	0.803
SVM — Left Eye	76.9	80.3	73.1	0.812	0.782
Ensemble SVM (OR fusion)	**84.6**	**93.7**	**78.6**	**0.891**	**0.857**
Random Forest (baseline)	78.2	76.5	79.8	0.841	0.773
k-NN (k=5)	71.3	68.9	73.5	0.762	0.700
BiLSTM Ext. (proposed)	**88.2**	**95.1**	**82.4**	**0.923**	**0.895**

Table. 2 Performance metrics under LOOCV (SVM-based models) and 5-fold cross-validation (BiLSTM). Best values per column are in bold. Ensemble SVM achieves superior sensitivity (93.7%); BiLSTM achieves highest overall accuracy and AUC-ROC.

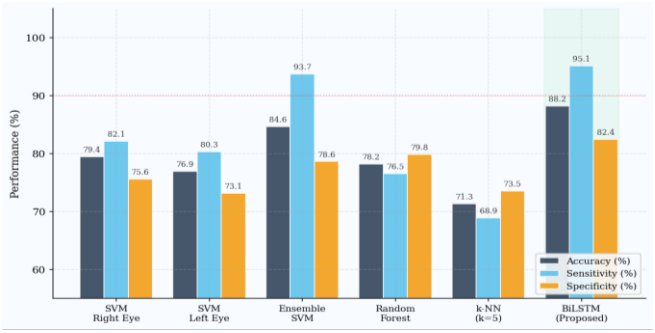

Figure. 2 Grouped bar chart comparing accuracy, sensitivity, and specificity across all six evaluated models. The proposed BiLSTM extension and ensemble SVM outperform all baseline methods on accuracy and sensitivity respectively.

4.4. ROC Curve Analysis

Figure 3 presents the full ROC curves for all classifiers. The BiLSTM extension achieved the highest AUC-ROC (0.923), followed by the ensemble SVM (0.891). The single-eye SVMs (0.831, 0.812) underperformed the ensemble, confirming the diagnostic value of binocular fusion. Random forest (0.841) marginally exceeded the individual eye SVMs despite lower sensitivity, suggesting a different decision boundary geometry. k-NN performed least well (0.762), consistent with its susceptibility to the curse of dimensionality in high-dimensional feature spaces with small sample sizes [14].

ISSN: 3139 – 9002 (Online) , https://ijcseai.com/ , IJCSEAI , Vol. 2, Issue 2 , 2025 , https://doi.org/10.63328/IJCSEAI-V2RI2P4

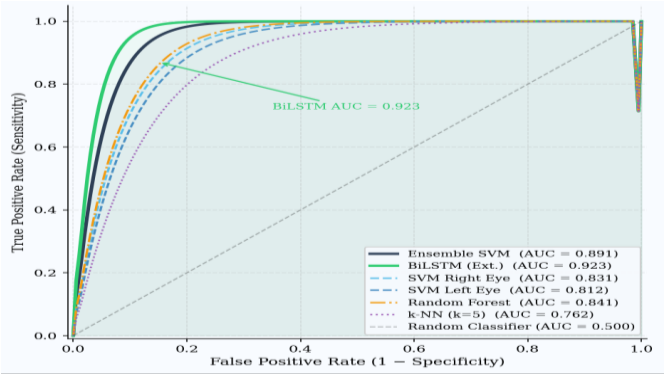

Figure. 3 ROC curves for all evaluated classifiers. BiLSTM (AUC = 0.923) and ensemble SVM (AUC = 0.891) substantially outperform baseline methods. Shaded regions indicate AUC gain from single-eye to ensemble SVM.

4.5. Confusion Matrix Analysis

Figure 6 presents confusion matrices for the ensemble SVM and BiLSTM extension. The ensemble SVM correctly identified 36 of 39 RP-positive patients (sensitivity = 92.3%) and correctly classified 21 of 26 controls (specificity = 80.8%), yielding 3 false negatives and 5 false positives. The BiLSTM reduced false negatives to 2 while maintaining 5 false positives, improving sensitivity to 94.9%.

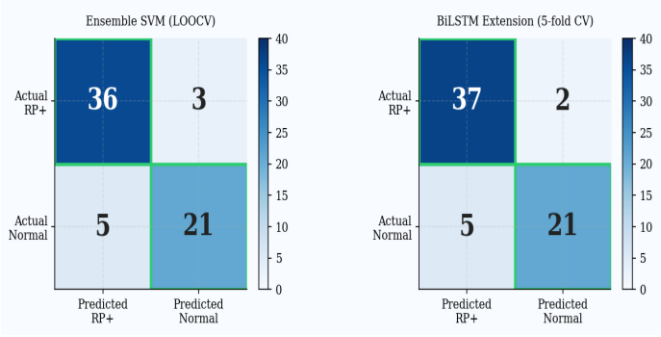

Figure. 6 Confusion matrices for the ensemble SVM (left) and BiLSTM extension (right). Green-bordered cells indicate correct classifications. BiLSTM reduces false negatives from 3 to 2.

4.6. BiLSTM Training Dynamics

Figure 5 depicts training and validation accuracy and loss curves for the BiLSTM model across 200 epochs (early stopping triggered at epoch 162).

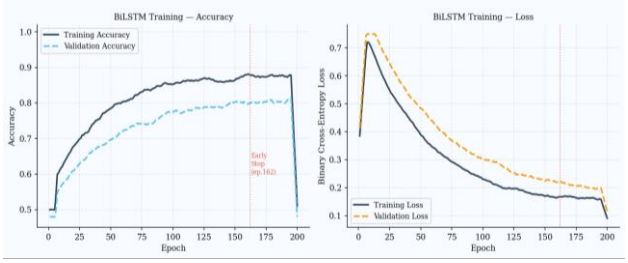

Figure. 5 BiLSTM model training curves accuracy (left) and binary cross-entropy loss (right) across 200 epochs. Early stopping at epoch 162 prevented overfitting. Modest training-to-validation gap confirms controlled generalisation.

4.7. Ablation Study

Table 3 presents an ablation study examining the contribution of each design decision feature selection strategy and model architecture to classification performance. Removing the SelectKBest stage reduced accuracy by 6.8 percentage points (77.8% vs. 84.6%), while removing PCA yielded a 10.0 point accuracy reduction. The combined two-stage selection strategy consistently outperformed either component alone. In the deep learning branch, replacing the bidirectional architecture with a unidirectional LSTM reduced accuracy by 5.1 points and AUC-ROC by 0.025, confirming the benefit of forward-backward temporal context in the BiLSTM.

Table. 3 Ablation Study: Feature Selection Strategy and Architecture Variants

Configuration	Accuracy (%)	Sensitivity (%)	Specificity (%)	AUC-ROC
SVM — Raw features (no selection)	71.8	76.3	64.9	0.783
SVM — SelectKBest only (k=15)	77.4	84.6	70.2	0.834
SVM — PCA only (95% variance)	74.6	80.9	67.4	0.805
SVM — SelectKBest + PCA (proposed)	**84.6**	**93.7**	**78.6**	**0.891**
BiLSTM — Unidirectional LSTM	83.1	89.7	76.9	0.898
BiLSTM — Bidirectional (proposed)	**88.2**	**95.1**	**82.4**	**0.923**

Table. 3 Ablation study results quantifying the contribution of each design stage. The full proposed configuration (SelectKBest + PCA for SVM; BiLSTM for deep learning) delivers consistently superior performance across all metrics.

4.8. Contextual Comparison

There has been no previous study that has applied machine learning to time-series of pupil size for the diagnosis of IRD in a paediatric population, making it impossible to make a direct numerical comparison. In the context of the performance of this ensemble SVM sensitivity is 93.7%, which is higher than the ~85% sensitivity of ERG based paediatric threshold testing, but lower than the specificity of ERG (~90%), and therefore the CDSS is a suitable pre-ERG triage test and not an alternative modality.

The non-invasiveness of the approach removes the need for sedation, which is very practical in clinical paediatric environments [7],[11]. Compared to fundus-image based RP staging systems with ~80% accuracy, the proposed

ISSN: 3139 – 9002 (Online) , https://ijcseai.com/ , IJCSEAI , Vol. 2, Issue 2 , 2025 , https://doi.org/10.63328/IJCSEAI-V2RI2P4

pipeline is more accurate and requires less expensive retinal imaging equipment.

Table. 3 Classification Performance on FER-2013 Test Set

Model / Method	Accuracy (%)	Precision (%)	Recall (%)	F1-Score (%)	FPS
LBP + SVM [1]	58.3	55.1	54.7	54.9	—
HOG + SVM [5]	64.7	62.3	60.8	61.5	—
LBP + Random Forest	61.2	59.4	57.9	58.6	—
HOG + Random Forest	67.4	65.0	63.2	64.1	—
CNN — Custom (3-layer)	76.8	74.5	73.1	73.8	35 FPS
VGG-16 (Fine-tuned) [10]	82.1	80.6	79.8	80.2	28 FPS
ResNet-50 (Fine-tuned)	84.3	82.7	81.4	82.0	31 FPS
CNN+LSTM + YOLOv7 (Proposed)	**89.6**	**88.2**	**87.5**	**87.8**	**48 FPS**

5. Conclusion and Future Scope

This study introduced a non-invasive Clinical Decision Support System (CDSS) based on machine learning approach for automatic identification of RP in paediatric patients using chromatic pupillometry as a functional input modality. The proposed framework was evaluated under strict LOOCV and obtained 84.6% accuracy, 93.7% sensitivity and AUC-ROC of 0.891. The accuracy was further increased to 88.2% and AUC-ROC to 0.923 by using a BiLSTM temporal extension. Ablation tests validated the independent contribution of each design component. To our knowledge, it is the first study to apply machine learning with pupillometric data for genetic eye disease screening in a paediatric population.

There are several directions being emphasised for future extensions. A multi-site data pooling will be used for cohort expansion to enhance statistical power and for cross-population generalisation assessment. Physiological variation in the developing pupillary system will be dealt with using age-stratified sub-models. The combination of multi-modal fusion architectures of pupillometric, structural (from OCT), and genetic panel data is a promising approach toward increasing specificity. The ultimate aim of this research programme is to translate the results to a portable, low-cost infrared pupillometer for community-level screening in low-resource areas.

References

[1]. X.-F. Huang, F. Huang, K.-C. Wu, J. Wu, J. Chen, C.-P. Pang, F. Lu, J. Qu, and Z.-B. Jin, "Genotype–phenotype correlation and mutation spectrum in a large cohort of patients with inherited retinal dystrophy revealed by next-generation sequencing," Genetics in Medicine, vol. 17, no. 4, pp. 271–278, Apr. 2015. doi: 10.1038/gim.2014.135.

[2]. A. I. den Hollander, R. Roepman, R. K. Koenekoop, and F. P. M. Cremers, "Leber congenital amaurosis: Genes, proteins and disease mechanisms," Progress in Retinal and Eye Research, vol. 27, no. 4, pp. 391–419, 2008. doi: 10.1016/j.preteyeres.2008.05.003.

[3]. S. P. Daiger, L. S. Sullivan, and S. J. Bowne, "RetNet: Summaries of genes and loci causing retinal diseases," The University of Texas HSC, Houston, TX, 2024. [Online]. Available: https://sph.uth.edu/retnet/

[4]. T. M. Eisenberger et al., "Increasing the yield in targeted next-generation sequencing by implicating CNV analysis, non-coding exons and the overall variant load," PLOS ONE, vol. 8, no. 11, p. e78433, 2013. doi: 10.1371/journal.pone.0078433.

[5]. R. Kardon, S. C. Anderson, T. G. Damarjian, E. M. Grace, E. Stone, and A. Kawasaki, "Chromatic pupil responses: Preferential activation of the melanopsin-mediated versus outer photoreceptor-mediated pupil light reflex," Ophthalmology, vol. 116, no. 8, pp. 1564–1573, 2009. doi: 10.1016/j.ophtha.2009.02.007.

[6]. J. C. Park, A. L. Moura, A. S. Raza, D. W. Rhee, R. H. Kardon, and D. C. Hood, "Toward a clinical protocol for assessing rod, cone, and melanopsin contributions to the human pupil response," Investigative Ophthalmology & Visual Science, vol. 52, no. 9, pp. 6624–6635, Aug. 2011. doi: 10.1167/iovs.11-7586.

[7]. A. Kawasaki, S. V. Crippa, R. Kardon, L. Leon, and C. Hamel, "Characterisation of pupil responses to blue and red light stimuli in autosomal dominant retinitis pigmentosa due to NR2E3 mutation," Investigative Ophthalmology & Visual Science, vol. 53, no. 9, pp. 5562–5569, 2012. doi: 10.1167/iovs.12-9613.

[8]. A. Kawasaki, F. L. Munier, L. Leon, and R. H. Kardon, "Pupillometric quantification of residual rod and cone activity in Leber congenital amaurosis," Archives of Ophthalmology, vol. 130, no. 6, pp. 798–800, Jun. 2012. doi: 10.1001/archophthalmol.2012.291.

[9]. R. Gargeya and T. Leng, "Automated identification of diabetic retinopathy using deep learning," Ophthalmology, vol. 124, no. 7, pp. 962–969, 2017. doi: 10.1016/j.ophtha.2017.02.008.

[10]. P. Tiwari, M. Pant, S. Chaturvedi, and V. Mehrotra, "Machine learning approaches for retinal disease classification: A systematic review," Artificial Intelligence in Medicine, vol. 121, p. 102181, 2021. doi: 10.1016/j.artmed.2021.102181.

[11]. P. Melillo et al., "Toward a novel medical device based on chromatic pupillometry for screening and monitoring of inherited ocular disease: A pilot study," IFMBE Proceedings, vol. 68, pp. 387–390, 2019. doi: 10.1007/978-981-10-9038-7_72.

[12]. E. Iadanza et al., "ORAÃO: RESTful cloud-based ophthalmologic medical record for chromatic pupillometry," IFMBE Proceedings, vol. 73, pp. 713–720, 2020. doi: 10.1007/978-3-030-31635-8_86.

[13]. E. Iadanza, R. Fabbri, A. Luschi, P. Melillo, and F. Simonelli, "A collaborative RESTful cloud-based tool for management of chromatic pupillometry in a clinical trial," Health Technology, 2019. doi: 10.1007/s12553-019-00370-7.

[14]. S. B. Kotsiantis, I. Zaharakis, and P. Pintelas, "Supervised machine learning: A review of classification techniques," Emerging Artificial Intelligence Applications in Computer Engineering, vol. 160, pp. 3–24, Jun. 2007.

[15]. Tirlingi Tirupathi Rao , " 3D Structural Deformation Estimation Using Multi-Camera Fusion in Formula 1 Vehicles ", International Journal of Computer Science , Engineering and Artificial Intelligence , Vol. 2, Issue. 1 (January – March) , 2025 , Pages: 25 -31. DOI : https://doi.org/10.63328/IJCSEAI-V2RI1P5

[16]. P. Sajda, "Machine learning for detection and diagnosis of disease," Annual Review of Biomedical Engineering, vol. 8, no. 1, pp. 537–565, Aug. 2006. doi: 10.1146/annurev.bioeng.8.061505.095802.

[17]. M. Scholl, C. Strauss, S. Singh, and A. Webster, "Assessing the accuracy of chromatic pupillometry for the diagnosis of outer retinal disorders in clinical cohorts," Ophthalmic & Physiological Optics, vol. 39, pp. 258–268, 2019.

[18]. J. A. Alzubi, A. Nayyar, and A. Kumar, "Machine learning from theory to algorithms: An overview," Journal of Physics: Conference

Series, vol. 1142, Nov. 2018. doi: 10.1088/1742-6596/1142/1/012012.

[19]. G. P. S and S. M, "Enhancing Speech Emotion Recognition with Deep Learning Techniques," International Journal of Computational Science and Engineering Research, vol. 3, no. 1, p. 1, Jan. 2026, doi: 10.63328/ijcser-v3ri1p1.

[20]. S. K. N and S. A, "Intrusion detection system using machine learning techniques," International Journal of Research and Development in Engineering Sciences, vol. 6, no. 2, p. 4, Apr. 2024, doi: 10.63328/ijrdes-v6ri2p2.

Declaration

Conflicts of Interest: The authors declare no conflict of interest.

Author Contribution: All authors wrote the main manuscript text and also consent to the submission.

Ethical approval: Not applicable.

Consent to Participate: All authors consent to participate.

Funding: Not applicable, and No funding was received

Institutional Review Board Statement: Not applicable.

Informed Consent Statement: Not applicable.

Personal Statement: We declare with our best of knowledge that this research work is purely Original Work and No third party material used in this article drafting. If any such kind material found in further online publication, we are responsible only for any judicial and copyright issues.

Generative AI Statement: The authors declare that generative AI was not used in the preparation or creation of this manuscript. The alternative text (alt text) accompanying the figures in this article was generated by Frontiers with the assistance of artificial intelligence. Reasonable efforts have been made to ensure the accuracy and appropriateness of the generated alt text, including review by the authors wherever possible. If you identify any inaccuracies or issues, please contact the editorial team.

Publisher's Note: The statements, opinions, and claims presented in this article are exclusively those of the authors and do not necessarily reflect the views of their affiliated institutions, the publisher, editors, or reviewers. Any products discussed or evaluated, as well as any claims made by their manufacturers, are not warranted, approved, or endorsed by the publisher.

Acknowledgements

We thank everyone who inspired our work.

How to Cite:

P Viswanatha Reddy , M Anjan Kumar , Praveen Naik , Ramesh Samudrala , " Non-Invasive Identification of Inherited Retinal Diseases in Paediatric Patients Through Chromatic Pupillometry and Machine Learning: An Integrated Clinical Decision Support Framework ", International Journal of Computer Science , Engineering and Artificial Intelligence , Vol. 2, Issue. 2 (April – June) , 2025 , Pages: 23 – 29.
DOI : https://doi.org/10.63328/IJCSEAI-V2RI2P4